



Cooperativity and Frustration in Protein-Mediated Parallel Actin Bundles

Homin Shin,¹ Kirstin R. Purdy Drew,² James R. Bartles,³ Gerard C.L. Wong,² and Gregory M. Grason¹

¹*Department of Polymer Science and Engineering, University of Massachusetts, Amherst, Massachusetts 01003, USA*

²*Department of Materials Science and Engineering, University of Illinois at Urbana-Champaign, Urbana, Illinois 61801, USA*

³*Department of Cell and Molecular Biology, Northwestern University, Feinberg School of Medicine, Chicago, Illinois 60611, USA*

(Received 17 September 2009; published 30 November 2009)

We examine the mechanism of bundling of cytoskeletal actin filaments by two representative bundling proteins, fascin and espin. Small-angle x-ray studies show that increased binding from linkers drives a systematic overtweak of actin filaments from their native state, which occurs in a linker-dependent fashion. Fascin bundles actin into a continuous spectrum of intermediate twist states, while espin only allows for untwisted actin filaments and fully overtweaked bundles. Based on a coarse-grained, statistical model of protein binding, we show that the interplay between binding geometry and the intrinsic flexibility of linkers mediates cooperative binding in the bundle. We attribute the respective continuous (discontinuous) bundling mechanisms of fascin (espin) to difference in the stiffness of linker bonds themselves.

DOI: 10.1103/PhysRevLett.103.238102

PACS numbers: 87.16.Ka, 82.35.Pq, 87.15.A-

Actin binding proteins (ABP's) that direct the assembly of *F*-actin cytoskeletal polymers are often divided into two classes: those that induce formation of networks, and those that induce formation of finite-sized parallel bundles [1]. These motifs have been observed for a variety of linkers, from ABP's to simple multivalent ions, and have been studied theoretically and experimentally [2–12]. Espin and fascin are two representative bundle-forming ABP's. Espins are found in mechanosensory microvilli and microvillar derivatives, while fascin is typically found in filopodia. Although the gross structure of the induced *F*-actin bundles are similar for espin and fascin [6,7], they behave differently, and serve cellular functions with different requirements. Here, we aim to explore a deeper taxonomy governing the different behaviors of bundle-forming ABP's.

In this Letter we demonstrate that while different cross-linkers ultimately drive parallel actin bundles to the same structural state, the thermodynamic transition to that state depends sensitively on linker stiffness. Monitoring the structural evolution of bundled filaments by small-angle x-ray scattering (SAXS), we find that increasing the ratio of fascin to actin leads to a continuous overtweaking of filaments from their native symmetry. In contrast, cross-linking by espin produces a coexistence of two populations, one with the fully overtweaked geometry, and one with native twist. We propose a coarse-grained lattice model of cross-linking in actin bundles to capture the interplay between filament and cross-linker flexibility as well the incommensurate geometries of actin filaments and fully cross-linked bundles. This model reveals that stiffness of cross-linking bonds and resistance to filament torsion sensitively control the level of cooperativity of cross-linking at different points along the filament. The mean-field thermodynamics of this model predicts: (1) a flexible linker regime allows a continuous increase of cross-links with increased chemical potential; (2) a stiff linker regime exhibits a highly cooperative and discontinuous linker

binding transition; and (3) a critical-end point separating these regimes. The respective continuous and discontinuous changes in filament overtweak measured by scattering can be correlated with the flexible linker and stiff linker regimes of the lattice model, where a similar response to increased cross-linking is predicted, suggesting that small differences in linker structure lead to qualitative differences in global phase behavior of the cytoskeleton.

To prepare x-ray samples, fresh *F*-actin was prepared from rabbit skeletal muscle *G*-actin monomer (Cytoskeleton, Inc.), polymerized by adding 100 mM KCl, and treated with human plasma gelsolin (Cytoskeleton, Inc.) and phalloidin to control average *F*-actin length ($\sim 1 \mu\text{m}$) and prevent depolymerization [13], respectively, using methods previously described [7]. Cross-linking proteins included recombinant rat espin 3A (34.3 kDa) and recombinant human fascin (57.8 kDa), which were expressed in bacteria with an *N* terminal $6 \times \text{His}$ tag, affinity purified under nondenaturing conditions and dialyzed into *E* buffer [7]. *F*-actin and cross-linking protein were mixed at specific molar ratios $R = N_{\text{crosslinker}}/N_{G\text{-actin}}$, with 0.15 mg *F*-actin, incubated, and centrifuged in sealed quartz capillaries. SAXS experiments were performed at 9 keV at beam line 4-2 of the Stanford Synchrotron Radiation Lightsource and at 12 keV at the BESSRC-CAT (beam line 12-ID) at the Advanced Photon Source. The scattered radiation was collected using an MAR Research CCD camera (pixel size = $79 \mu\text{m}$). The sample-to-detector distances are set such that the q -range is $0.01 < q < 0.2 \text{ \AA}^{-1}$, where $q = (4\pi \sin\theta)/\lambda$, λ is the x-ray wavelength, and 2θ is the scattering angle. The 2D SAXS data from both beam lines have been checked for mutual consistency. As described previously [7], the twist of the actin filaments when bundled with cross-linking proteins was determined by fitting 2D SAXS data to the four sphere model of variably-twisted *F* actin convolved with the bundle structure factor [4,14].

The structure of espin-actin and fascin-actin bundles has been previously investigated [6,7,15–17], although the thermodynamic phase behavior of these actin +ABP systems has not been mapped out. SAXS data for F actin condensed by fascin or espin are presented in Fig. 1. The circularly averaged peak positions of the hexagonally coordinated fascin-actin bundle are similar to those of the espin-actin bundles. Peaks were found at 0.057, 0.100, 0.120, 0.134 \AA^{-1} for both espin and fascin mediated bundles at high R , with the first two corresponding to the interactin structure factor peaks, and the latter corresponding to intra-actin helical layer line peaks. The interactin spacing for the fascin-actin bundles obtained from the position of the q_{10} peak [most intense peak visible in Figs. 1(a) and 1(b)] was equal to $4\pi/(\sqrt{3}q_{10}) = 12.9 \pm 0.3$ nm, slightly larger than that of espin-actin bundles, 12.6 ± 0.2 nm [7]. This corresponds to a fascin size of 5.4 ± 0.3 nm, and an espin size of 5.1 ± 0.2 nm using an F -actin diameter of 7.5 nm [18]. Using the 4-sphere model, we found that the position of the espin-actin bundle layer lines indicated a F -actin overtwist of 0.9 ± 0.2 degrees from the native left-handed 13/6 monomers/turn twist symmetry of unbundled F actin to a symmetry of 28/13 monomers/turn [7]. Furthermore, at low R , coexisting bundled and unbundled phases are observed in the espin-actin system, as in Fig. 1(d) at $R = 0.05$ where broad 13/6 layer line peaks at 0.114 and 0.125 \AA^{-1} can be observed simultaneously with sharp Gaussian peaks of the overtwisted hexagonal bundles. This 2-phase coexistence in the espin-actin bundle data, and constant layer line peak position in strong contrast to the small, systematic shift of the first layer line peak of the fascin-actin bundles towards higher q observed with increasing R [Fig. 1(c)]. This systematic shift in peak position is only visible in the layer line peaks of the fascin-actin system, and not in the interactin structure factor peaks, indicating that it is the F -actin twist which is gradually increasing from the native F -actin unbundled twist symmetry (13/6 monomers/turn) with increasing fascin concentration, with a maximum of ~ 0.9 degrees of overtwist at high R , in agreement with recent measurements [6,17]. The contrast in twisting be-

havior for espin and fascin mediated bundles is summarized in Fig. 1(e). This fascin-actin bundle data show a similar decrease in twist with decreasing fascin concentration to that previously published [6]. Espin-cross-linked actin exhibits a jump between coexisting “low” and “high” twist states with increasing espin concentration via a first order transition, while fascin-cross-linked actin exhibits gradual twist changes from low to high twist with increasing fascin concentration, suggesting a continuous thermodynamic pathway.

To study cross-linking thermodynamics, we introduce a coarse-grained lattice model reflecting the intrinsic geometrical frustration of parallel actin bundles. The helical axes of actin filaments are positioned at the vertices of a hexagonal lattice with spacing D . The helical configuration of G -actin monomers in each filament is described by a set of X, Y “spins” on planes spaced along the backbone of the filament, as pictured in Fig. 2. The i th monomer is then represented by a spin vector $a\hat{S}_i$, where a is the monomer size. The positions described by these vectors serve as a proxy for the locations of binding sites on the monomers themselves. For the native configuration of actin filaments with 13/6 symmetry, the spins wind around the filament axis by $\omega_0 = 12\pi/13$ per monomer [see Fig. 2(a)].

We introduce a Hamiltonian, described by a set of spins for filament configurations, as well as the binding site occupancy n_{ij} between two monomers, i and j , separated by a distance Δ_{ij} ,

$$\mathcal{H}_{\text{binding}} = \sum_{ij} n_{ij} \left[-\epsilon_0 + \frac{k}{2} (\Delta_{ij} - \Delta_0)^2 \right], \quad (1)$$

where the sum runs over sites on neighboring filaments and n_{ij} equals 0 or 1. Here ϵ_0 describes the minimum (distortion free) energy of optimal binding and k the stiffness of linkers, defining the energy cost to deform the linkers from an aligned state, $\Delta_{ij} = \Delta_0$. In this model, we consider the in-plane cross-links so that the square deformation has a rather simple form, $(\Delta_{ij} - \Delta_0)^2 \approx C_0 - 2a^2 \hat{\mathbf{D}}_{ij} \cdot (\hat{S}_i - \hat{S}_j) + \mathcal{O}(S^2)$, where $\hat{\mathbf{D}}_{ij}$ is the unit vector of a lattice direction. Hence, protein cross-linking occurs more favor-

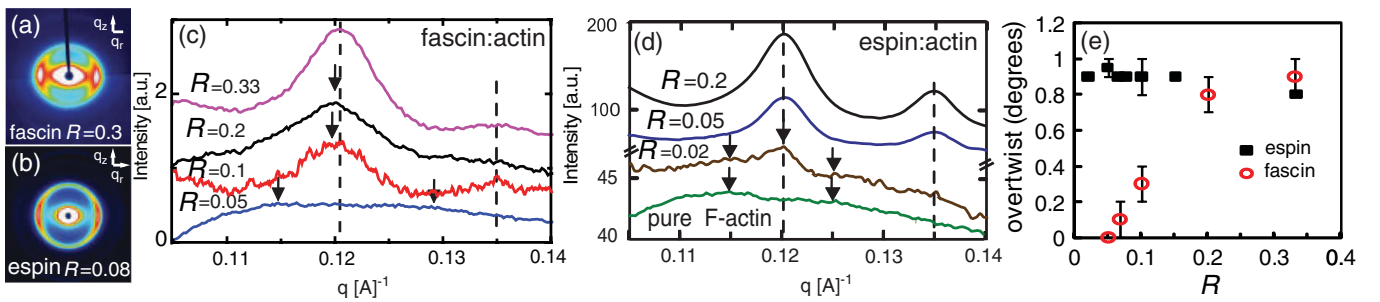


FIG. 1 (color). Experimental evidence of first and second order twisting transitions. 2D SAXS images of (a) fascin-actin bundles and (b) espin-actin bundles. Circularly averaged SAXS data showing first and second layer line peaks for (c) fascin-actin bundles and (d) espin-actin bundles [7] as a function of R . Data is shown with a pseudo-Voigt background subtraction. Arrows show position of first layer line peak maximum in (c) and the position of the unbundled layer line peaks at 0.114 and 0.125 \AA^{-1} . (e) Measured twist of actin bundles as a function of R .

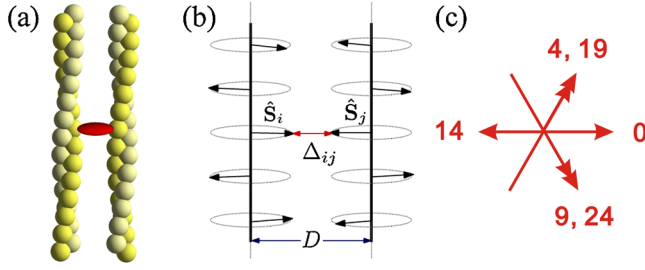


FIG. 2 (color online). (a) A schematic picture of two actin filaments linked by a cross-link. (b) G-actin monomers in filaments are represented by a set of X, Y spins. (c) The top view of the angular distribution of cross-linkers (red arrows) in the unit cell of 28/13 ground state.

ably where two monomers co-orient along the directions of the lattice packing. Based on this model we predict that a unique regular structure maximizes the number of perfectly aligned cross-links/monomer in the bundle, while requiring minimal distortion of the intrinsic twist of the filament [19]. The structure is composed of 4 sections of 5-monomers with 30/14 (overtwisted) symmetry and 2 sections of 4-monomers with 24/11 (undertwisted) symmetry, so that 6 monomers/repeat align perfectly with sixfold lattice directions and all bonds from neighboring filaments are coincident. This structure fulfills an overall repeat unit of 28 monomers per 13 turns, consistent with the overtwisted 28/13 geometry observed by scattering. Based on an exhaustive search, we have found that hexagonal tilings of alternative composite structures of up to 40 monomers/ repeat—including the corresponding 13/6 structure—have smaller fraction of bound monomers than $6/28 \approx 0.214$, provided by the composite 28/13 geometry.

The conformational adjustments of filaments required for optimal binding give rise to cooperative cross-linking, mediated by torsional fluctuations of filament and linker flexibility. To demonstrate this, we adopt a continuum model for twist distortions, given by angular deviations from the native filament geometry, $\mathcal{H}_0 = \frac{C}{2} \sum_{\ell} (\Delta\phi_{\ell} - \omega_0)^2$, where ℓ denotes the vertical layer, C is the torsional stiffness and $\Delta\phi_{\ell} = \phi_{\ell} - \phi_{\ell-1}$ is the azimuthal angle difference between two adjacent monomers along the filament. Based on the geometric distortion of bonds the energy for adding a bond at a layer ℓ can be written as, $-\epsilon_0 + U(1 - \cos[\phi_{\ell} - \phi_m])$. Here, (ℓ, m) label the vertical and angular position of bonds, and $\phi_m = 2\pi m/6$ indicates the preferred sixfold direction of monomer orientation. U is a measure of linker flexibility, $U \approx ka^2$. In our model the 28/13 ground state packing maximizes the number of coincident monomers from neighboring filaments, allowing a particular large number of favorable cross-links to form. There are six monomers in a repeat unit of 28 monomers, which are $(0, 0)$; $(4, 1)$; $(9, -1)$; $(14, 3)$; $(19, 1)$ and $(24, -1)$ [see Fig. 2(c)].

Given a distribution of cross-linkers, we integrate out the spin degrees of freedom via a thermodynamic perturbation theory. To lowest order this yields an effective Hamiltonian

in terms of cross-links alone,

$$\mathcal{H}_{\text{eff}} \approx -\sum_{\ell} n_{\ell,m} \epsilon'_0 - \frac{1}{2} \sum_{\ell, \ell'} n_{\ell,m} V(\ell, \ell') n_{\ell',m'}, \quad (2)$$

where $\epsilon'_0 = \epsilon_0 - U/2$. $V(\ell, \ell')$ is a pairwise coupling between cross-linking of different monomers along a filament,

$$V(\ell, \ell') = \frac{\beta U^2}{2} \cos[\omega_0(\ell - \ell')] - 2\pi(m - m')/6 e^{-|\ell - \ell'|/\xi_t}. \quad (3)$$

Here $\xi_t = 2\beta C$ is the twist persistence length, over which the orientational correlations of the native filament geometry are “washed out” by torsional fluctuations. This van der Waals-like coupling of distinct bonds reflects statistical correlations in cross-linking along a filament. The rigidity of a cross-linking bond at layer ℓ pins the filament in an orientation where certain nearby monomers are close to their most favorable binding direction, so that $V(\ell, \ell') > 0$. Hence, the range and strength of $V(\ell, \ell')$ are determined by ξ_t and U , respectively.

We analyze the mean-field thermodynamics within the grand canonical ensemble at fixed chemical potential, μ , which regulates the cost of removing a cross-linking protein from solution. Assuming the sites of the ground state are occupied with a mean probability $\langle n_{\ell,m} \rangle = \rho$, the mean-field equation of state is determined by the solution to the self-consistency condition, $\rho = (1 + z^{-1} e^{-u\rho})^{-1}$. Here, $z = \exp[\beta(\mu + \epsilon'_0)]$ is the effective fugacity of cross-links, proportional to the concentration of unbound linkers in solution, and u is a measure

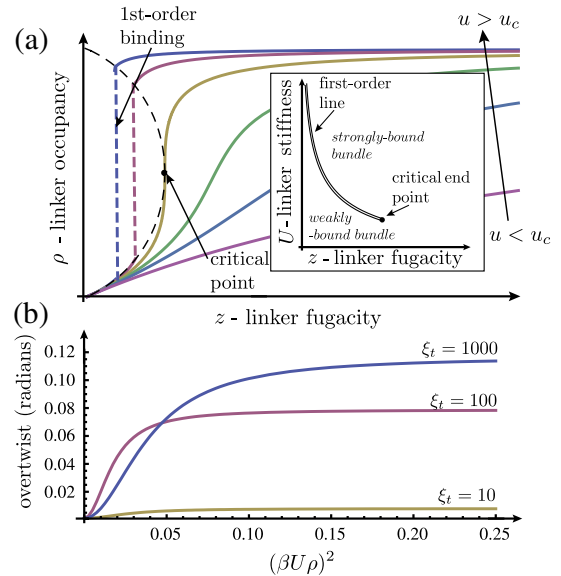


FIG. 3 (color online). (a) The predicted dependence of the mean site occupancy ρ on linker fugacity. The inset shows the phase diagram for fixed z and U . (b) The correlation between overtwist measured by $\text{Im}[\ln g]$ and ρ for given values of ξ_t .

of the net cooperativity of cross-linking. Specifically, $u = N_b^{-1} \beta \sum_{\ell \neq \ell'} V(\ell, \ell')$ where the sum is carried out over the total N_b possible sites in the 28/13 ground state along a single filament. While cooperativity monotonically increases with linker stiffness, $u \propto (\beta U)^2$, this parameter has a more complex dependence on torsional rigidity. For small ξ_t , cooperative binding only occurs over short distances, so that $u \sim \xi_t$. At larger values of ξ_t the incommensurability between the native 13/6 and 28/13 twist symmetries requires significant distortions of either the filaments or the bonds between them. The incommensurate effects at long range lead to a reduction of u at large ξ_t and maximum value around $\xi_t \approx 60$.

The predicted mean-field equation of state is shown in Fig. 3. For low cooperativity, $u < u_c = 4$, ρ is a continuously increasing function of z , as cross-linking at distinct sites occurs largely independently in this regime. Increasing linker stiffness increases the correlations in binding events, as indicated by the rise in maximum linker susceptibility, $\chi_\rho = d\rho/dz$, for larger u . At the critical point $u = u_c$, this susceptibility diverges at $\rho = 1/2$, $\chi_\rho \sim |z - z_c|^{-2/3}$, indicating a second order transition. For $u > u_c$, in which the stiff links enhance the cooperative interactions, the transition becomes first order with a discontinuous jump in linker density that increases with u . Owing to the Ising symmetry of \mathcal{H}_{eff} , this model possesses a phase diagram for fixed z and U reminiscent of a “liquid-vapor” transition, in which a line of first order transitions terminates at a critical end point (see Fig. 3). Note that the value of the critical point implies a critical stiffness of order $k_c \approx k_B T/a^2$.

A second result of this analysis is one-to-one correspondence between mean occupancy of linker sites in bundles and filament overtwist observed in our SAXS measurements. We analyze the following monomer-monomer correlation function, $g(\ell_0) \equiv \langle \exp[i(\phi_{\ell_0 + \delta\ell} - \phi_{\ell_0} - \omega_0 \delta\ell)] \rangle$, where the factor in the exponential is the excess angle between a monomer at ℓ_0 and the next monomer $\ell_0 + \delta\ell$ in 28-monomer packing relative to the native 13/6 twist, that is, the mean overtwist between neighboring bonds. We calculate $g(\ell_0)$ perturbatively to $\mathcal{O}(U^2)$ for the given ground state and find overtwist, as measured by $\text{Im}[\text{In}g]$, to be continuously increasing function of ρ for any given values of linker and filament stiffness [see Fig. 3(b)]. Indeed, because neighboring pairs of occupied bonds exert a torque on the filament to align monomers to the ground state symmetry, it can be shown that $\text{Im}[\text{In}g] \sim \rho^2$ in the $U \rightarrow 0$ limit. Hence, the continuous (discontinuous) increase in cross-linking binding with increasing linker fugacity, implies a simultaneous continuous (discontinuous) structural transition in terms of filament twist.

Theoretical results here suggest that *F*-actin cross-linking in parallel bundles is acutely sensitive to cross-linker flexibility. Both predicted regimes are experimentally observed. The continuous dependence of actin filament overtwist on the concentration of fascin, suggests that

these linkers are too flexible to exhibit a critical binding transition. The comparative insensitivity of overtwist on linker concentration in espin bundles suggests that this binding occurs as a highly cooperative transition, in which the rigidity of linkers immediately drives the bundle into the fully saturated and overtwisted state. The difference between espin and fascin binding suggests fundamental differences in the mechanism of bundle formation (twist, diameter, rigidity), which correlates to the distinct physiological functions of the respective actin bundles. Hair cells require structurally identical actin bundles in order to mediate reproducible mechano-chemical transduction. This may be facilitated by an actin + crosslinker system in which the same bundle structure is induced for a range of espin-actin molar ratios. In contrast, fascin’s function is to organize cytoskeletal bundles in filopodial protrusions under a diverse set of mechanical conditions [20], a task that may be facilitated by the broad range of binding states and a sensitive dependence on the fascin-actin ratio. This view is consistent with *in vivo* observations of filopodial bundles that are weakly bound and highly dynamic [21].

H. S. and G. M. G. acknowledge the support from UMass, Amherst through a Healey Endowment Grant and thank the Aspen Center for Physics for its hospitality. G. W. is supported by NSF DMR08-04363 and the RPI-UIUC NSEC; J. B. is supported by NIH DC004314 and the Hugh Knolwes Center. Part of this work is conducted at the UIUC Frederick Seitz MRL, the Advanced Photon Source, and the Stanford Synchrotron Radiation Lightsource.

-
- [1] B. Alberts *et al.*, *Molecular Biology of the Cell* (Taylor and Francis, New York, 2002).
 - [2] R. Tharman *et al.*, Proc. Natl. Acad. Sci. U.S.A. **103**, 13974 (2006).
 - [3] O. Pelletier *et al.*, Phys. Rev. Lett. **91**, 148102 (2003).
 - [4] T. E. Angelini *et al.*, Eur. Phys. J. E **16**, 389 (2005).
 - [5] G. C. L. Wong *et al.*, Phys. Rev. Lett. **91**, 018103 (2003).
 - [6] M. M. A. E. Claessens *et al.*, Proc. Natl. Acad. Sci. U.S.A. **105**, 8819 (2008).
 - [7] K. R. Purdy *et al.*, Phys. Rev. Lett. **98**, 058105 (2007).
 - [8] G. M. Grason and R. F. Bruinsma, Phys. Rev. Lett. **99**, 098101 (2007).
 - [9] B. -Y. Ha and A. J. Liu, Phys. Rev. Lett. **81**, 1011 (1998).
 - [10] M. J. Stevens, Phys. Rev. Lett. **82**, 101 (1999).
 - [11] L. Haviv *et al.*, Eur. Biophys. J. **37**, 447 (2008).
 - [12] N. S. Gov, Phys. Rev. E **78**, 011916 (2008).
 - [13] P. A. Janmey *et al.*, J. Biol. Chem. **261**, 8357 (1986).
 - [14] H. Al-Khayat *et al.*, J. Mol. Biol. **252**, 611 (1995).
 - [15] L. Tilney *et al.*, J. Cell Biol. **86**, 244 (1980).
 - [16] J. R. Bartles, Curr. Opin. Cell Biol. **12**, 72 (2000).
 - [17] D. J. Derosier and R. Censullo, J. Mol. Biol. **146**, 77 (1981).
 - [18] K. C. Holmes *et al.*, Nature (London) **347**, 44 (1990).
 - [19] H. Shin and G. M. Grason (to be published).
 - [20] J. Faix and K. Rottner, Curr. Opin. Cell Biol. **18**, 18 (2006).
 - [21] Y. S. Aratyn *et al.*, Mol. Biol. Cell **18**, 3928 (2007).